Gamma Knife® Stereotactic Radiosurgery and Hypo-Fractionated Stereotactic Radiotherapy

45

Dheerendra Prasad

Learning Objectives

- Understand the technology and technique of Gamma Knife radiosurgery.
- Develop a framework for planning a radiosurgery case.
- Understand dose prescription guidelines and the key Gamma Knife literature supporting them.

Description and Evolution of Modality

Swedish neurosurgeon, Lars Leksell, proposed the concept of stereotactic radiosurgery [1] as the use of stereotactically directed ionizing beams to ablate intracranial targets in 1951. Sixteen years later, together with physicist Börje Larsson [2], he completed the design of the Leksell Gamma Knife(LGK) as a dedicated tool to perform brain radiosurgery. The LGK in all its various models consists of a number of independent Co^{60} sources that emit gamma radiation in the 1.1 MeV range that are focused through a series of collimators to one focal point (isocenter). The diameter of the isovolume created by the cross-firing of approximately 200 beams can be varied from 4 to 16 mm (18 mm in the early models). Treatment plans are generated by superimposing multiple such dose clouds creating a multi-isocenter dose plan. The target is then stereotactically aligned with the focal point of the unit, and treatment delivery is one isocenter at a time.

The key features of the LGK and the evolution of the technology over the various models are summarized in Fig. 45.1.

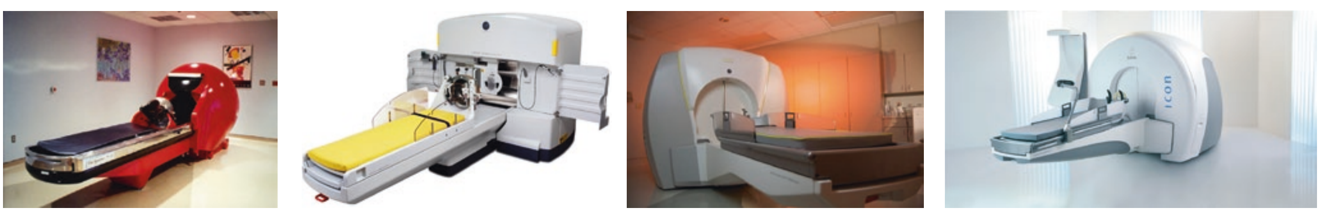

Model U

- Brought the technology to USA
- Totally manual device
- Core idea of fixed target fixed source

Model 4C

- Robotic auto positioning of patient
- Semi-automated
- Core idea of fixed target fixed source
- Allowed increased conformaliity of plans by making it easy to traet multiple isocenters

Prefexion

- Auto positioning plus auto collimation switching
- Fully automated
- Core idea of fixed target fixed source
- Further improvement in conformality and plan quality with use of sectors
- Enhanced radiation safety

Icon

- Integrated imaging and frame and frameless option
- Fully automated
- Core idea of fixed target fixed source
- Permits new workflows
- Onboard imaging and patient motion monitoring with gating

Fig. 45.1 Key technological highlights for various models of the Leksell Gamma Knife arranged chronologically from left to right

D. Prasad
Department of Radiation Medicine and Neurosurgery, Roswell Park Comprehensive Cancer Center, Buffalo, NY, USA
e-mail: d.prasad@roswellpark.org

E. L. Chang et al. (eds.), *Adult CNS Radiation Oncology*, https://doi.org/10.1007/978-3-319-42878-9_45

Immobilization Techniques and Image Guidance

Precise delivery of the treatment plan is dependent on the ability of the system to localize the target in stereotactic coordinate space. This requires immobilization of the patient. There are two immobilization techniques that can be used with the LGK: the Leksell stereotactic frame and a thermoplastic mask.

Leksell Stereotactic Frame

Originally designed for stereotactic neurosurgery, this device is made of high-grade anodized aluminum and uses a Cartesian coordinate system to localize targets in stereotactic space (Fig. 45.2). The coordinates are expressed as a triplet of *x*, *y*, and *z*. The origin of the coordinate system (0,0,0) is on the right—superior—posterior aspect of the skull. The *x*-axis runs from the right to the left; the *y*-axis runs from posterior to anterior and the *z*-axis from superior to inferior. The center of the coordinate system has a value of 100,100,100.

Using the frame provides a very high level of accuracy allowing the device to perform at its calibrated specification which is always better than 0.3 mm. Inaccuracy in imaging and frame displacement as a result of improper application are the major sources of error with this setup.

Thermoplastic Mask

With the LGK Icon®, it is possible to immobilize the patient using thermoplastic mask and a deformable at cushion (Fig. 45.3). This fixation system permits single as well as hypo-fractionated stereotactic treatments with the Gamma Knife. Stereotactic coordinates are obtained by performing a cone beam computerized tomography (CBCT) using the onboard CBCT system.

Cone Beam CT

The CBCT in the ICON is integrated into the patient positioning and source unit as one rigid entity. This makes it operate in true Leksell coordinate space—and every voxel in the reconstructed image has known Leksell coordinates, requiring a transformation along only the *z*-axis, while determining true *x* and *y* coordinates. This distinguishes it from all other image guidance systems in use. The unit operates at two different computerized tomography dose index (CTDI) settings 2.5 mGy and 6.3 mGy. It is customary to use the higher CTDI setting for the localizing scan when the co-registration is being performed to a pre-planning MRI, allowing more detail for mutual information matching. The lower CTDI setting is used for the daily delivery CBCT which is co-registered to the reference CT.

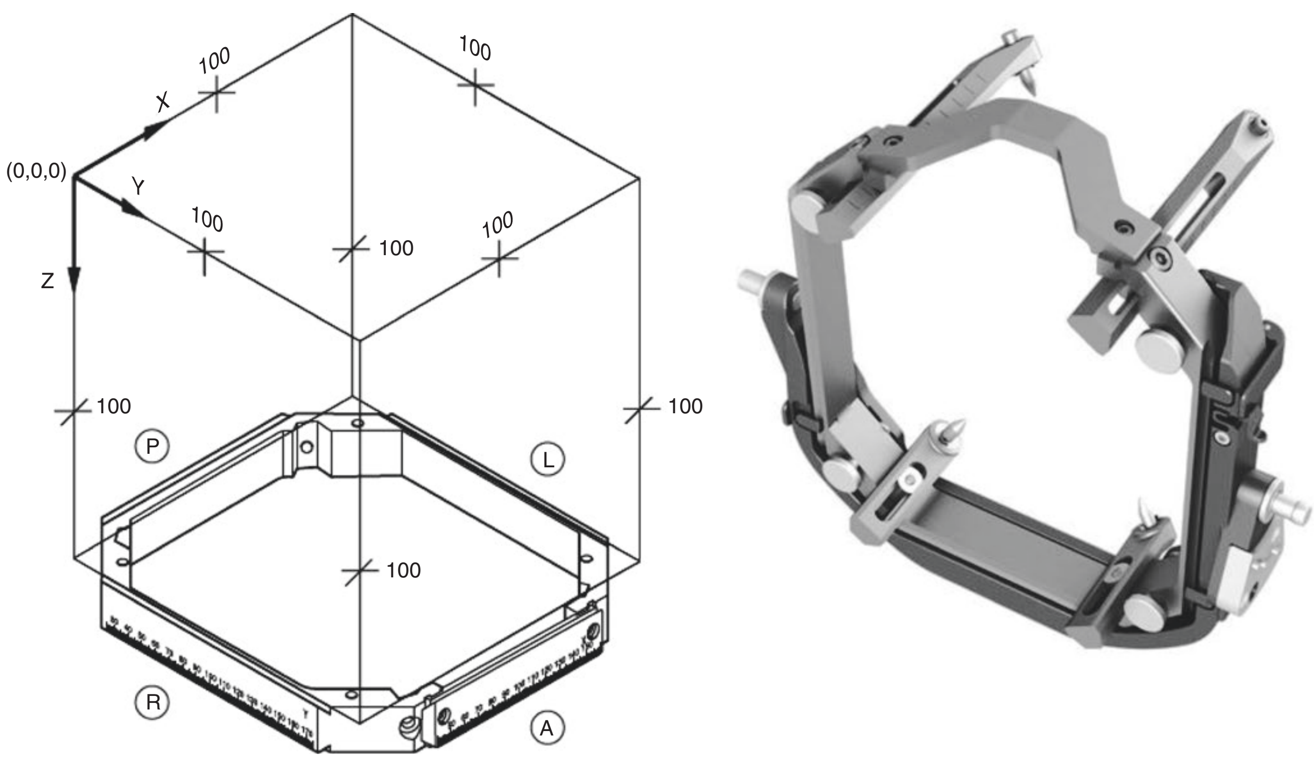

Fig. 45.2 Leksell coordinate space and the Leksell stereotactic frame model G. [Courtesy of Elekta]

Accuracy of the CBCT system has been verified experimentally (Dalhalwi) and shows excellent concordance with frame-based coordinates in phantom studies. Insert error values here.

Intra-Fraction Motion Management

In order to ensure "intra-fraction patient position" when a thermoplastic mask is in use, a high-definition motion management system (HDMM) is coupled with the thermoplastic mask (Fig. 45.4). The HDMM uses an infrared reflective marker placed on the nose and tracked by an infrared camera relative to static reflectors located on the patient head cradle. A motion trace for the marker is then displayed on the operator console allowing the operator to set a tolerance level for the maximum deviation of the patient from the initial position. The system automatically suspends (gates) delivery of radiation if the patient exceeds the programmed tolerance. Should the patient return within tolerance in a predefined time interval, treatment delivery will continue; however, if the patient remains out of position for a single or repeated periods exceeding 20 s, then the treatment is interrupted and the patient is ejected from the machine. The operator then decides whether to override the deviation or to perform a new cone beam CT and realign the patient for continued delivery. In practice with a cooperative patient, it is not unusual to have deviations of the nasal marker less than 0.5 mm. Most patients can be delivered to treatment with nose marker deviations under 1.5 mm. It should be pointed out that the marker on the nose is a surrogate for target position, and the relative target deviation depends on target location in the brain. Based on studies conducted on a test system, the corresponding deviation at the target was on average half of that displayed as the nose marker deviation.

Fig. 45.3 Thermoplastic mask, moldable cushion, and cradle for hypo-fractionated treatments. [Courtesy of Elekta]

Treatment Planning

Treatment planning for the LGK is performed on a dedicated planning system—Leksell Gamma Plan®—and can be performed manually, semiautomatically as a forward plan with optimization assistance or as a fully automated inverse plan.

At the outset, it is important to understand that the treatment planning with LGK is more akin to brachytherapy rather than a conventional external beam plan. This is due to the fact that the plan is often multi-isocenter and comprised of multiple superimposed dose clouds, each with its own iso-

Fig. 45.4 High-definition motion management for mask-based delivery with the LGK Icon®. [Courtesy of Elekta]

center called a "shot" in LGK parlance. The goal is to create a confluent dose cloud that conformally encloses the target. This fundamental aspect of an LGK plan makes it inherently more conformal but also more prone to heterogeneity. Another key difference from traditional IMRT and SRS plans on a LINAC-based system is the fact that dose is prescribed (or normalized) to isodose lines varying from 90% to 30% (with the mode and median prescription IDL in plans being the 50%). This derives from the fact that the LGK dose profile offers the steepest dose gradient between the 40% and 55% isodose lines based on its physical design characteristics.

Typical Dose Distribution

At initial loading, LGK houses upward of 6000 curies of radioactivity and a resultant dose rate of 3.3–3.6 Gy/min. Based on the collimator output factors, this dose rate is modified by a factor of 0.8–1.0 for the three collimators 4, 8, and 16 mm. Their numeric designation refers to the diameter in mm of the 80% isovolume of a single shot of a given size. Dose profiles are shown in Figs. 45.5 and 45.6, and typical dose distributions of the three collimators as depicted in Gamma Plan are shown in Fig. 45.7.

In practice the user has to develop a sense for the isovolume generated by each collimator in three dimensions; since visual inspection is dependent on the magnification of the images being viewed, it is best to start by placing a test shot of a given size on the images in question.

When more than one isocenter/shot is present, the superimposed distribution depends on the size of collimators used and the separation between the isocenters. It is common practice to place adjacent shots such that they are overlapping. As shown in Fig. 45.8, the inter-isocenter distance has an effect on both the prescription isodose (yellow) and the appearance of cold and hot spots.

For the Perfexion and Icon models, sources are mounted in groups of 24 on movable conical sections called sectors. Each of the 8 sectors for a given isocenter can be configured to be blocked or open and collimated to the 4, 8, or 16 setting. Since the sectors are arranged along the *z*-axis, the most intuitive effect of blocking a single sector is in the axial (*x*–*y*) plane. The influence on the other planes is not intuitive and is illustrated in Fig. 45.9 since in those planes the skull geometry affects the dose rate from different sectors differently. In addition to choosing the size of the collimation, sector blocks and composite shots (with different collimator settings for different sectors) are other ways to creating shaped dose distributions.

Prescriptions for the LGK were historically normalized to the 50% IDL, but in fact as the more automated models of LGK became available and the number of isocenters used

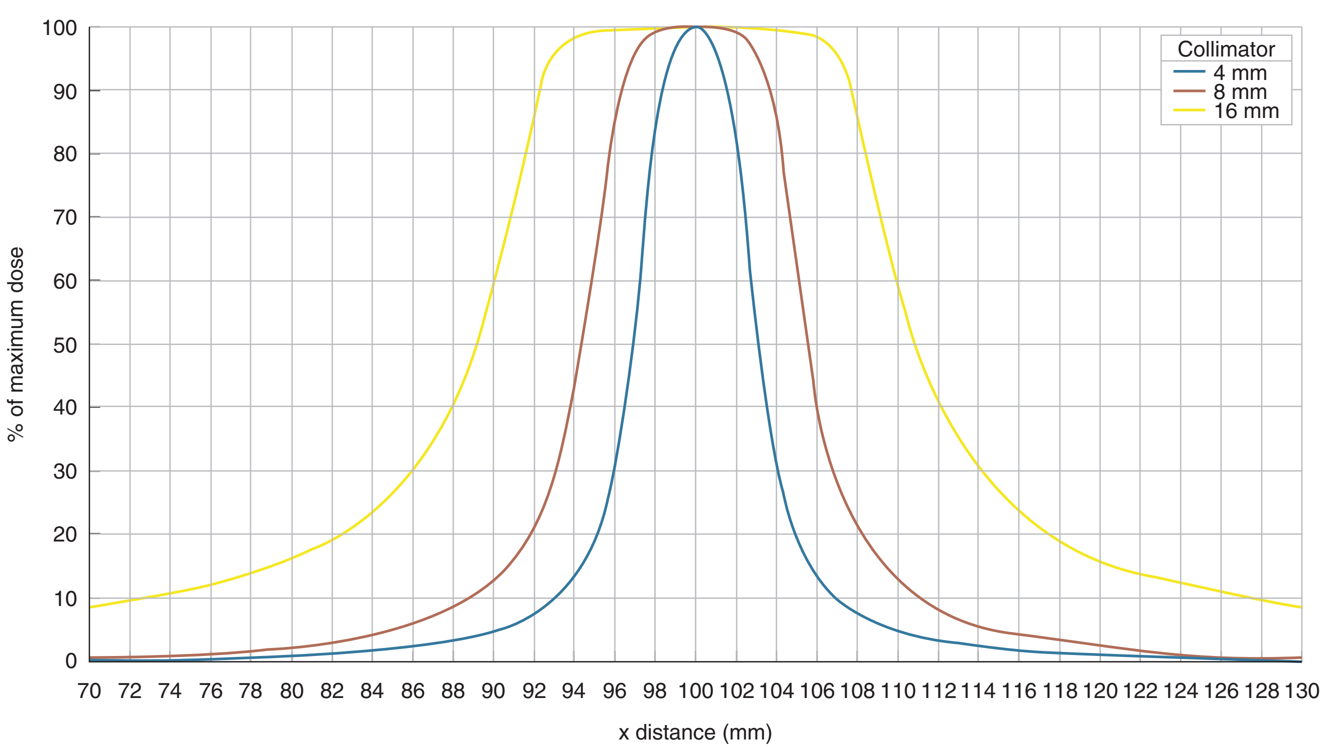

Fig. 45.5 Dose profiles along x-axis for the three collimators 4, 8, and 16 mm for LGK Perfexion and ICON

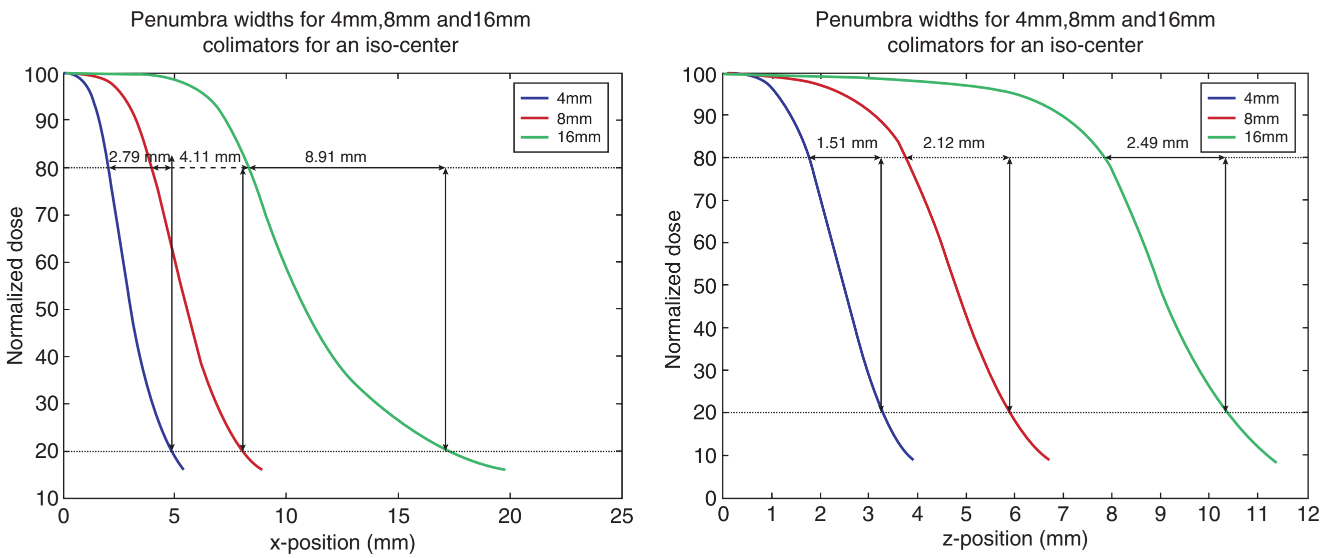

Fig. 45.6 Penumbra widths for all sources combined for Leksell Gamma Knife Perfexion or ICON

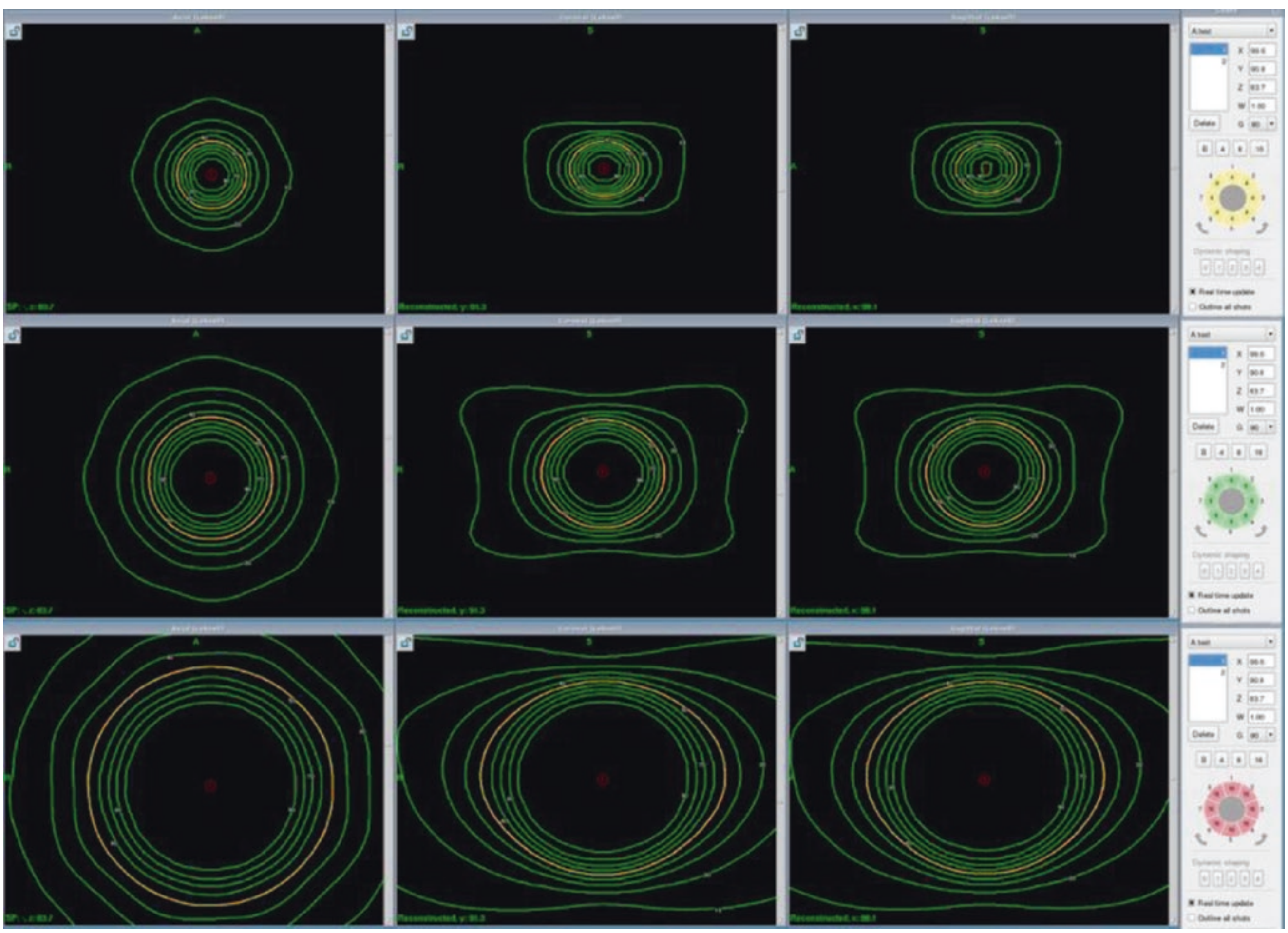

Fig. 45.7 Typical dose distribution of single 4, 8, and 16 mm collimators. The isodose line in yellow is the 50%. Also represented are 10, 20, 30, 40, 60, 70, 80, and 90% isodose lines in green, axial plan is represented in the left-most column, coronal in the middle column, and sagittal in the right-most column

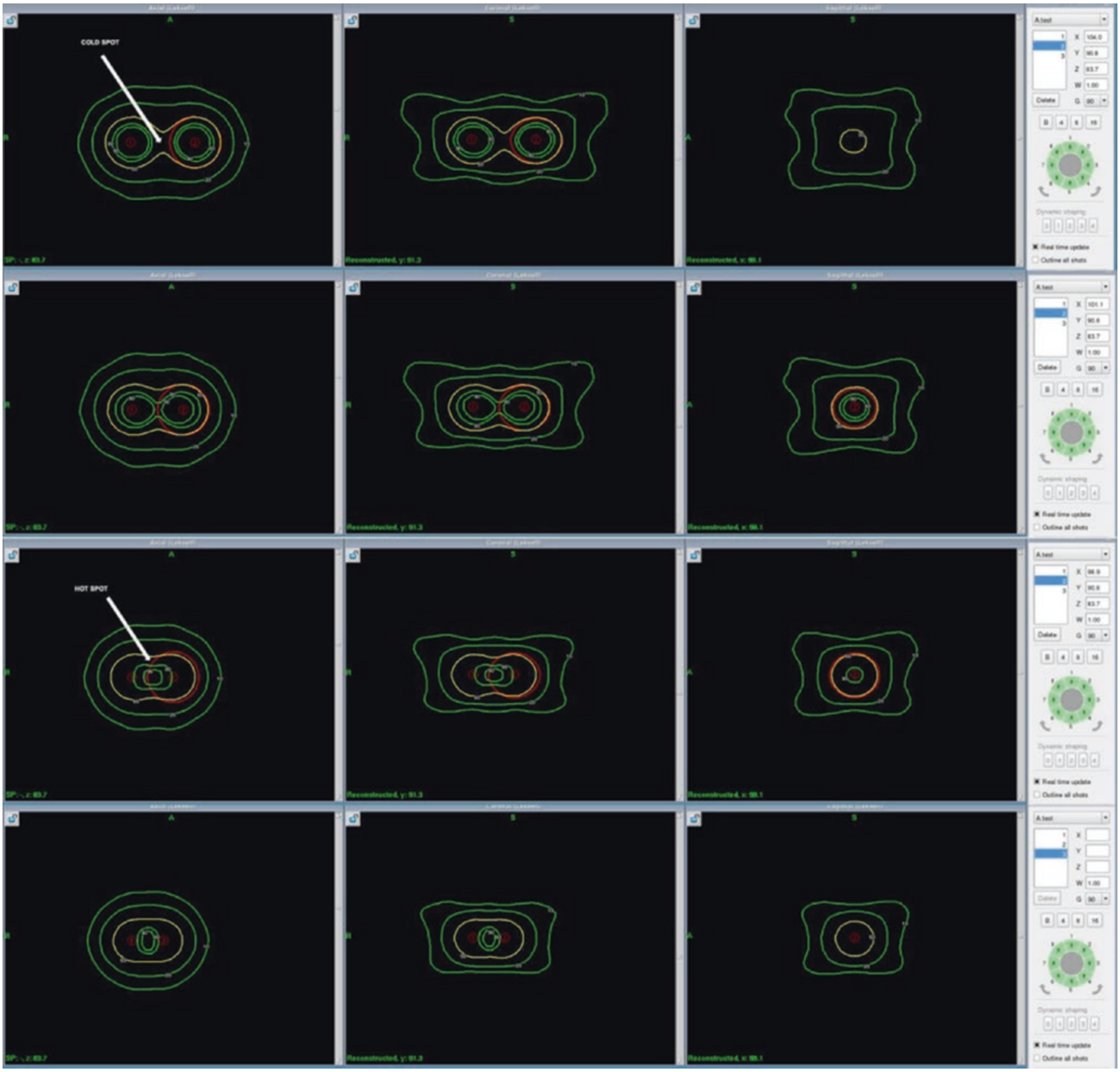

Fig. 45.8 Two 8 mm collimator shots placed adjacent to each other will yield a resultant dose distribution with a cold spot if they are non-overlapping. As they are moved closer (top to bottom), the cold spot diminishes in size, and a hot spot appears, axial plan is represented in the left-most column, coronal in the middle column, and saggital in the right-most column

increased, this is no longer true. Once multiple isocenter penumbras are combined, the steepest gradient can actually fall anywhere in the 40–55% IDL range. As discussed later this effect will reflect itself in steeper dose gradients and lower values of gradient index with normalization to less than 50% IDL. Care must be exercised in recognizing that the associated peak dose prescription and mean energy delivered by the plan will increase (Fig. 45.10). This can have consequences on the target and its response to the treatment.

Measures of Plan Quality

Before discussing planning and prescribing techniques with the LGK, it is important to discuss and define the parameters used to assess the quality of a dose plan.

Coverage: is defined as the proportion of the target volume (TV) that is covered by the prescription isodose volume (PIV), that is, Volume (PIV∩TV)/Volume (TV).

Selectivity: is defined as the proportion of the prescription isodose volume (PIV) that is inside the target volume (TV), that is, Volume (PIV∩TV)/Volume (PIV).

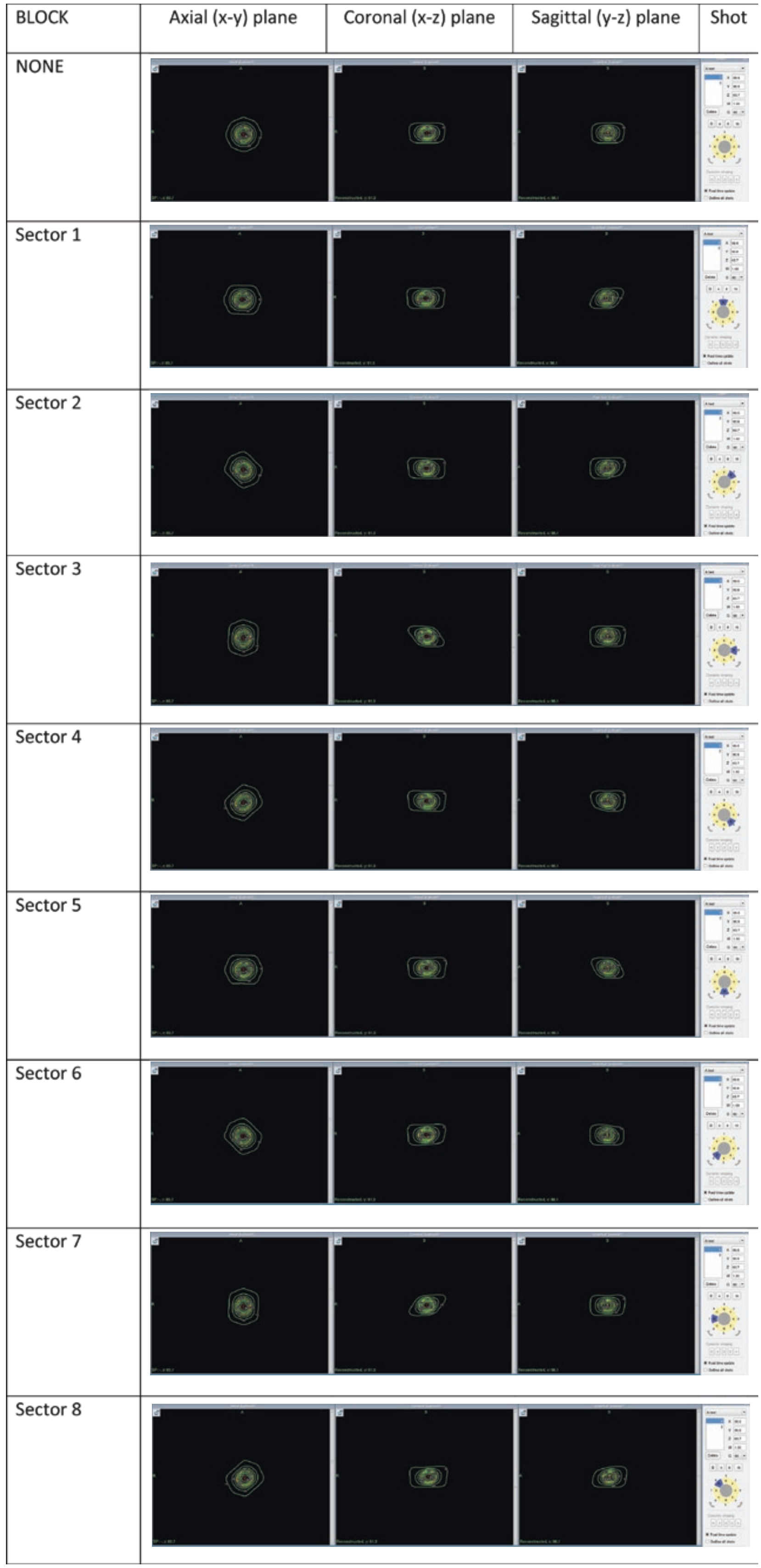

Fig. 45.9 Influence of sector blocking on the dose distribution from a 4 mm collimator, illustrating the difference between sectors

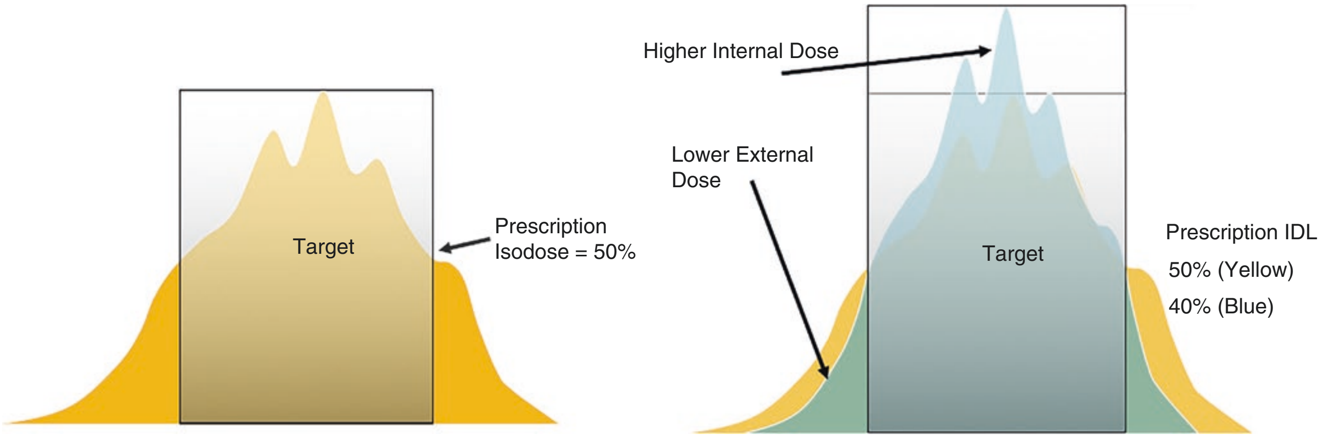

Fig. 45.10 Dose profile along the long axis of a tumor demonstrating the impact of renormalization of the dose plan from the 50% IDL to the 40% IDL: steeper gradient in normal tissue and elevated hot spot in target. [Courtesy of Ian Paddick]

Fig. 45.11 Dependence of the gradient index value on the prescription isodose line chosen

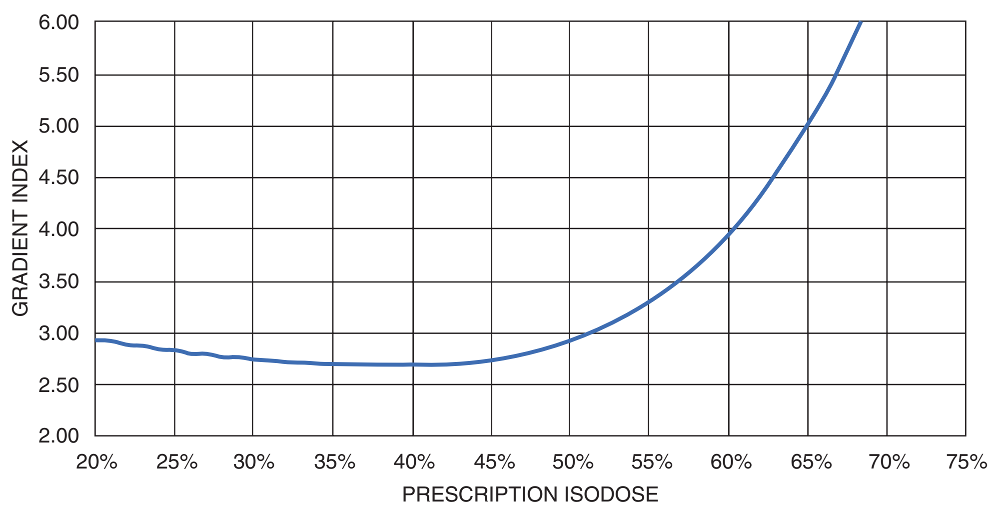

Gradient Index: is defined [3] as the quotient between the half-prescription isodose volume size and the prescription isodose volume size, that is, Volume (PIV25%)/Volume (PIV50%) if the planning isodose is 50%. Gradient index is commonly used to quantify the steepness of the dose falloff.

In addition, there are several measures of plan conformality:

RTOG PITV ratio: Defined by Shaw et al. [4], this is simply the ratio given by PIV/TV. It has the advantages of being easy to calculate. A value of >1 suggests a treatment volume that exceeds the target and implies irradiation of non-target surrounding tissue.

A value of <1 suggests a that treatment volume is smaller than the target and therefore indicates under-coverage of target. However, this ratio fails to reflect the actual overlap of the two volumes, leaving that determination to the planner.

Paddick conformity index: Defined by Paddick [5] this is calculated as the product of the coverage and selectivity. It is therefore $((PIV \cap TV)^2)/(PIV \times TV)$. It has a theoretical maximum value of 1. This index has the advantage of accounting for the concordance between dose and target as well as being a number that ranges from 0 to 1.

When designing a dose plan, the planner strives to achieve coverage as close to 1 as possible, although in most clinical situations, any value greater than 0.95 is found to be acceptable. Likewise, selectivity should be maximized, and values in 0.75 are easy to achieve and a reasonable target for the plan. Coverage and selectivity are often inversely related to each other, particularly in irreglar targets. Clinical judgment should be exercised to decide the balance between the two, as long as a minimum of 0.95 in coverage has been achieved.

The achievable gradient index (GI) has a theoretical limit based on the physical characteristics of the LGK around a value of 2.5. The factors that determine the GI include number and size of collimators used as well as the IDL to which the dose is prescribed. For example, in the curve shown in Fig. 45.11 based on one plan shows that the lowest GI would correspond to the 40% IDL. In addition to the global dose gradient, local gradients close to critical structures are also important for treatment plan quality assessment.

Forward Planning

The process of forward planning begins by delineating a target volume and designating it as such in the planning system. The user then sets a dose grid (called target or matrix) centered on the desired target. There is a separate grid on each target in the dose plan such as in multiple metastases.

The dose plan is then constructed by placing individual shots of varying collimator size and or composite shots in the target. The dose filling strategy varies greatly by operator and both "center out" and "periphery in" filling paradigms are used. In general, while the largest collimator provides the most coverage, it can also provide the sloppiest dose gradient in normal tissue. Thus, an efficient dose plan includes large collimators used away from critical structures and smaller collimators closer to critical structures. Fig. 45.12 demonstrates the construction of a dose plan for a cavernous sinus meningioma.

Optimizer-Assisted Forward Planning

The optimizer provided with LGP uses a cost function for optimization. The values of this cost function lie between 0 and 1, and the higher the value, the better the plan quality. The equation for the cost function is:

$$F = \frac{c^{\min(2\alpha,1)} s^{\min((2-2\alpha),1)} + \beta G + \gamma T}{1 + \beta + \gamma}$$

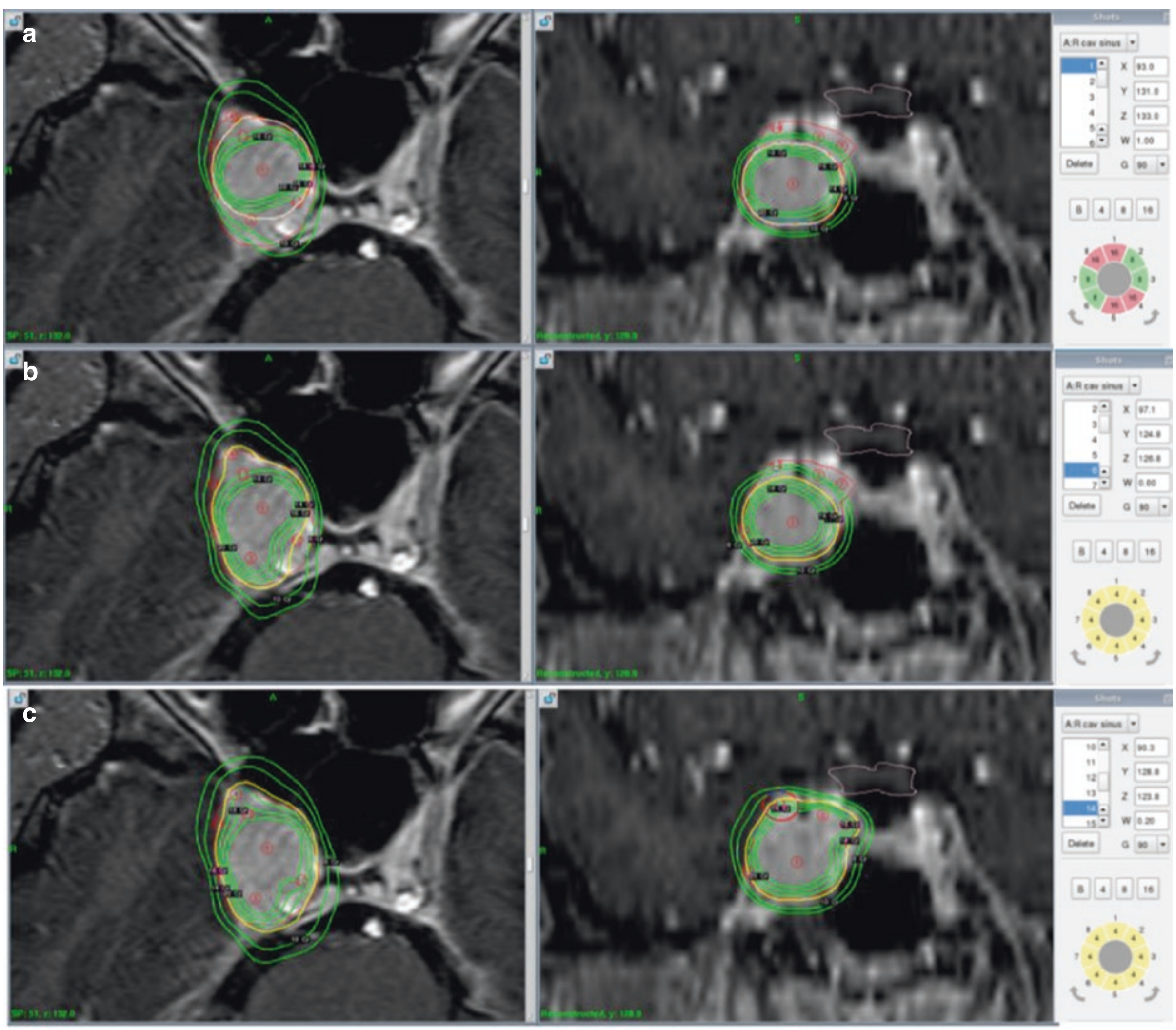

Fig. 45.12 Development of a forward dose plan for a right cavernous sinus meningioma. The plan begins (**a**) with the a composite 8 and 16 mm shot placed in the center of the tumor (shown are the axial, coronal, and shot configuration representations of the plan), followed by the addition of other shots (**b** and **c**) and the final dose plan in axial and coronal views (**d**) and sagittal and 3D representations (**e**). Note that doses are depicted in Gy. The isodose lines represented in green from outside in are 8, 10, 16, 18, and 20 Gy. The prescription line is 14 Gy shown in yellow. Target volume – red and optic chiasm and pathway (pink)

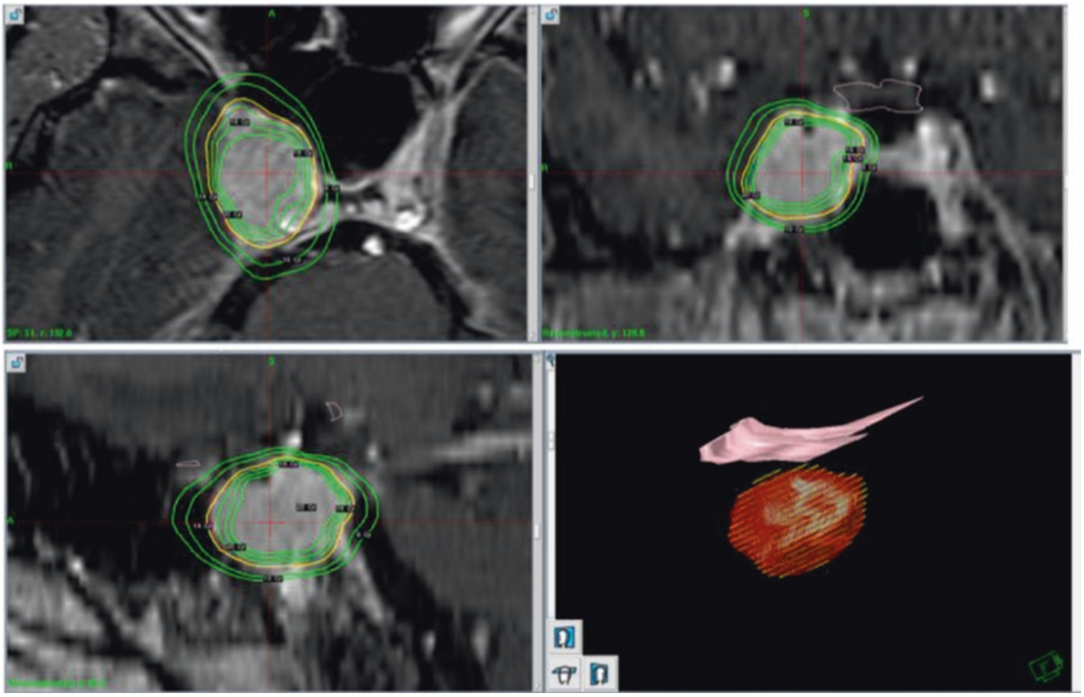

Fig. 45.12 (continued)

c is the target coverage, and *s* is the selectivity (defined previously).

α, β, and γ are weights between 0 and 1, set by the user.

G and *T* are functions whose values lie between 0 and 1 that describe how "good" the gradient index, *g*, and treatment time, *t*, are. ($G = 1$ if $g < 2.6$, $G = 0$ if $g > 6$ & $T = 1$ if $t < 0.25\ T_0$, $T = 0$ if $T > 1.5\ T_0$, where T_0 is the beam-on time at the start of the optimization).

α, β, and γ are set by the user with interactive sliders in the inverse planning settings dialog box (Fig. 45.13). The coverage and selectivity sliders are interconnected since they visually reflect the effect of the α parameter which drives the c and s variables in the cost function. The gradient index slider is the β parameter and drives the G parameter. Beam-on time represents the γ parameter and drives the T function.

Default settings in LGP are $\alpha = 0.5$, $\beta = 0.25$, and $\gamma = 0$. Therefore, if no changes are made, then the cost function ignores the time of plan delivery and concentrates on a good balance of selectivity and coverage with a gradient index which is as low as possible. The algorithm for optimization can change the already placed shots by the user and can even delete shots that are deemed redundant, using simulated annealing to maximize the cost function. The user can restrict the system from changing the manual plan in various ways. It is recommended that optimization be performed on a plan copy. If the lock positions and lock collimator settings boxes are checked (Fig. 45.13), then the only possible changes to the plan that the optimizer can make are shot weights. It is unlikely that this strategy will yield a big improvement in the plan. When only "lock collimator settings" is checked, the planning system will optimize the position and weights of the shots and will weight shots that are not necessary to zero.

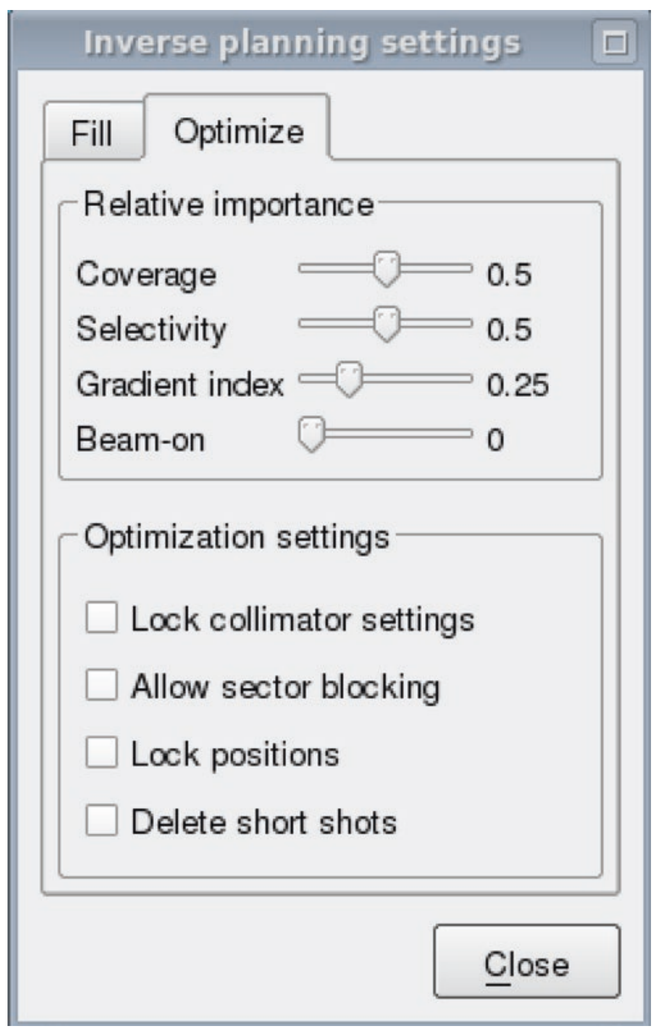

Fig. 45.13 Options in the inverse planning dialog for Leksell Gamma Plan

This is perhaps the most useful setting for small to mid-size targets where the planner is seeking to optimally place a few shots. It is possible to use this function repeatedly at various stages of the plan as one places for instance different size collimators. When no boxes are checked, the optimizer will introduce composite shots, and while the global dose gradient may improve, the user should evaluate the result with the lower isodose lines displayed so as to prevent locally sloppy gradients in high-risk areas since the optimizer does not take into account avoidance structures. At this stage, no sectors (other than those that were manually blocked by the user) will be blocked by the optimizer. Allowing sector blocking enables that functionality. It is important to reiterate that sector blocking usually negatively impacts gradient – as does normalization to a higher isodose line.

Choosing optimization parameters is often a personal matter and depends on the manner in which the shots are placed by the user and the individualized planning goals for the case in question. Table 45.1 enumerates typical settings for various targets.

Inverse Planning

Inverse planning requires no a priori placement of shots and uses the fill function of the program before using the optimization techniques described above. The fill dialog (Fig. 45.14) has a few options. The user can choose to use composite collimators or simple collimators. By unchecking the composite box, the dialog changes to display the 3 collimators 16, 8, and 4 and allows the user to decide which collimators are likely to best suit the plan intent.

If composite collimators are allowed, then the software uses the size slider as a guide to choosing composite sectors.

Table 45.1 Optimizer settings for various targets to obtain the best results with inverse planning with Gamma Plan

	Optimizer settings			Optimizer solution		
Target	Coverage /Selectivity	Gradient index	Time	Acceptable coverage	Acceptable selectivity	Acceptable gradient
Vestibular schwannoma	0.5/0.5	0.25–0.4	0	> 0.95	> 0.85	2.5–2.8
Cavern. Sinus meningioma	0.5/0.5	0.25–0.4	0	> 0.95	> 0.85	2.5–2.8
Convexity meningioma	0.6/0.4	0.25	0.3	> 0.95	> 0.7	2.5–3.2
Atypical meningioma	0.8/0.2	0.25	0.3	>0.95	>0.6	2.5–4
Large metastasis	0.7/0.3	0.25	0.2	>0.95	>0.6	2.5–4
Small metastasis	0.6/0.4	0.25	0	1	>0.6	3–7[a]
Surgical cavity-metastatic	0.7/0.3	0.25	0.2	>0.95	>0.6	2.5–4

[a]Often prescribed to isodose lines higher than 50% and therefore the achievable gradient index is higher

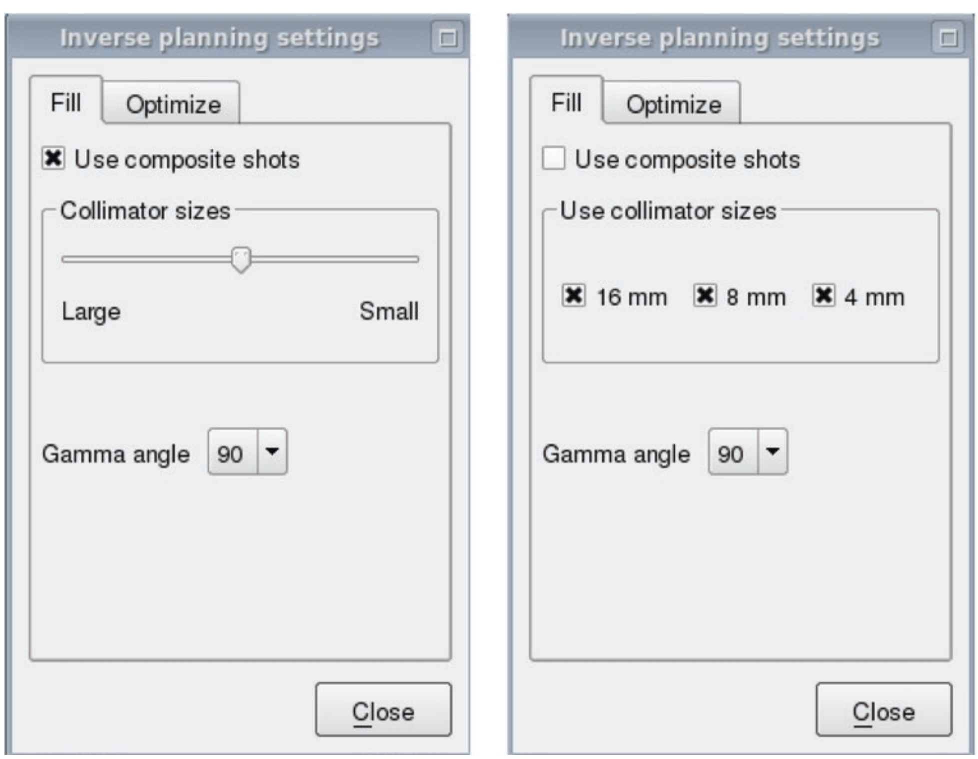

Fig. 45.14 The fill dialog

If set to small, then there are unlikely to be size 16 sectors in the placed shots. The program uses a bevy of preconfigured shot templates to fill, starting from the periphery and then populating the center. It initially places the shots without overlap of their 50% isovolume. The final setting is the gamma angle that can be chosen for patient docking based on lesion location and frame placement to avoid collisions (only usable with the stereotactic frame). Once shot filling is completed, the optimizer is used to optimize the dose plan as described in the previous section. Finally, manual placement of shots and or manipulation of the existing shots may be required to complete the process.

Dose Specification

Traditionally dose prescriptions with the LGK are defined as the minimum dose or dose to the margin of the target along with the percent IDL to which it is normalized. The corresponding maximum and mean doses while recorded are not used in publications when discussing efficacy and side effects. The exception to this pattern are functional targets where it is customary to prescribe the maximum dose to a point (given dose). Care must be taken not to confuse the two approaches to prescription.

Single Session: SRS

The doses used in single session radiosurgery are well worked out in LGK literature, and representative range is presented in Table 45.2. The outcomes of GKRS for vestibular schwannoma (Table 45.3), meningioma (Table 45.4), and metastatic tumors (Table 45.5) are provided for reference.

Table 45.2 Representative single session dose ranges by pathology

Diagnosis	Dose in Gy (Modal prescription)	References
Vestibular schwannoma	11–13 (12)	[6–18]
Meningioma	10–20 (15)	[19–49]
Pituitary adenoma: Nonsecretory	12–17 (15)	[24, 50–57]
Pituitary adenoma: Secretory	22–28	[24, 50–57]
Craniopharyngioma	10–15	[24, 58–61]
Low grade astrocytoma	12–15	[24, 62–68]
High-grade glioma	17–20	[68–72]
Metastatic tumor	16–24	[24, 73–92]
Metastatic tumor plus whole brain RT	16–18	[24, 73–92]
Glomus tumor	15	[93–96]
Other cranial schwannomas	12–14	[97–105]
Chordoma/Chondrosarcoma	17–22	[106]

Table 45.3 Outcomes for vestibular schwannomas treated with single-fraction GKRS

Study	Number of patients	% with local control	% Facial nerve morbidity	% Loss of hearing
Lunsford [6]	829	97	1	21
Regis [7]	1000	97	1.3	22
Landy [8]	34	97	0	0
Rowe [9]	234	92	1	25
Iwai [10]	51	96	0	41
Unger [11]	100	96	2	45
Litvack [12]	134	97	0	38
Petit [13]	45	96	0	12
Bertallanfy [14]	32	91	12.5	21
Prasad [15]	153	92	2	35
Lis˘c˘ák [16]	122	96	1.9	17
Kwon [17]	63	95	5	33
Norén [18]	669	95	2	30

Table 45.4 Tumor control rates for radiosurgery for meningiomas

Series	Cases	Control %
Bir et al. [37]	136	98
Bledso e et al. [26]	116	99
Choi et al. [27]	20	73
Chung et al. [28]	80	92
Davidson et al. [29]	36	95
DiBiase et al. [38]	137	86
Feigl et al. [39]	211	86
Franzin et al. [30]	123	91
Hasegawa et al. [31]	119	87
Jo et al. [32]	69	100
Kano et al. [40]	272	96
Kondziolka et al. [33]	488	95
Kreil et al. [41]	200	99
Massager et al. [34]	120	93
Metellus et al. [35]	36	94
Park et al. [42]	74	98
Park et al. [43]	39	92
Pollock et al. [36]	416	96
Sheehan et al. [44]	575	81
Shin et al. [45]	36	91
Starke et al. [46]	255	99
Williams et al. [47]	138	100
Zada et al. [48]	116	100
Zenonos et al. [49]	23	91

Multisession SRS (Hypo-Fractionated SRT)

With the introduction of the LGK Icon, it has become more practical to perform multisession SRS (hypo-fractionated SRT), although frame-based hypo-fractionation has been

Table 45.5 Outcomes for metastatic tumors treated with single session SRS with GK

Study	Number of patients	Tumor control rate (%)	Origin
Gerosa et al. [73]	225	88	All
Shiau et al. [74]	100	77	All
Kim et al. [75]	77	85	Lung carcinoma
Wowra et al. [24, 76]	126	89	All
Mori et al. [77]	60	88	Melanoma
Mori et al. [78]	35	90	Renal cell
Seung et al. [79]	55	89	Melanoma
Chen et al. [80]	190	89	All
Muacevic et al. [81]	56	83	All
Sneed et al. [82]	105	71	All
Lavine et al. [83]	45	97	Melanoma
Sansur et al. [84]	173	82	All
Amendola et al. [85]	68	94	Breast cancer
Simonova et al. [86]	237	91	All
Schöggl et al. [87]	67	95	All
Firlik et al. [88]	30	93	Breast cancer
Sheehan et al. [89]	273	84	Lung cancer
Muacevic et al. [90]	151	94	Breast cancer
Lippitz et al. 2004 [91]	15	89	All
Mix et al. [92]	214	87	Breast

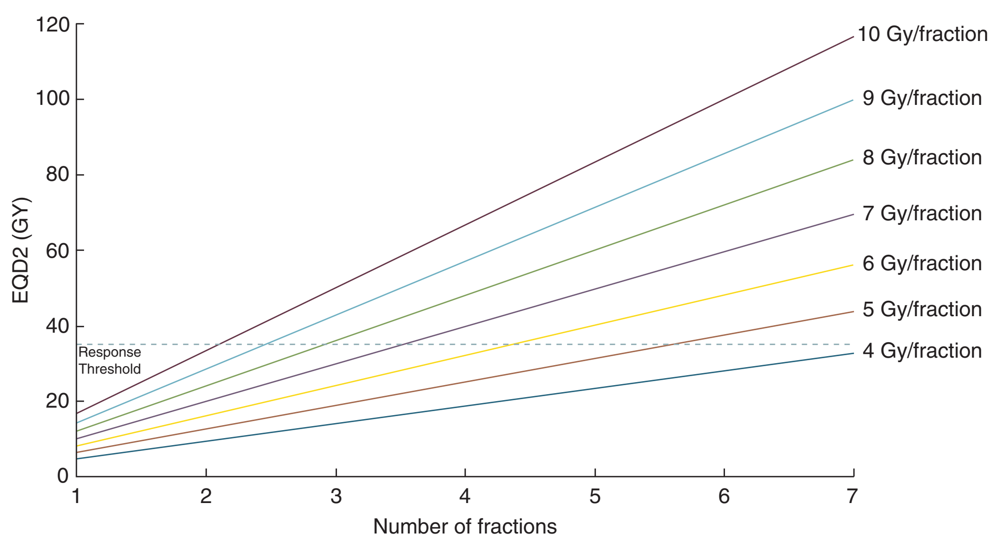

Fig. 45.15 Threshold EQD2 based on Martens et al. [108] for local control plotted against different fractionation schemes

performed both with the traditional frame and the Extend® frame.

Using the extend system, McTyre et al. [107] reported 34 cases where they used hypo-fractionation for benign tumors >10 cc in volume or abutting the optic pathway, vestibular schwannoma with the intent of hearing preservation, or a tumor previously irradiated with single-fraction GKRS.

The most challenging aspect of hypo-fractionation is developing an understanding of iso-effective doses with different fractionation schemes in the face of limited literature. One approach is to calculate the equivalent dose in 2 Gy fractions used in standard fractionation the EQD2. Martens et al. [108] reported a significant difference in median LC 14.9 months for EQD2 > 35 Gy and 3.4 months for EQD2 ≤ 35 Gy($p < 0.004$). In order to allow the reader a quick tool to decide the number and size of fractional doses that will exceed this threshold, Fig. 45.15 is useful.

In single session, the threshold EQD2 dose is exceeded by a dose of 17 Gy, but it takes 2 fractions of 10 Gy, 3 of 8 Gy, and so on to achieve the same EQD2. In more general terms, the most common doses used in treating metastatic tumors can be plotted against the EQD2 for various dose fractionation schemes as shown in Fig. 45.16.

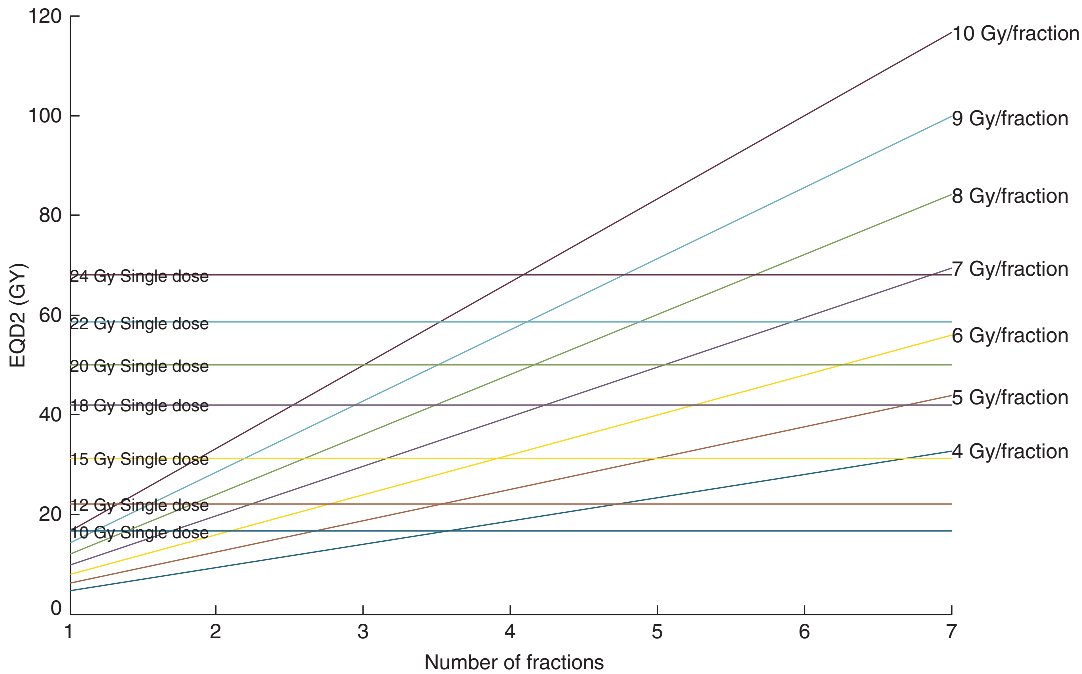

Fig. 45.16 Single doses commonly used for treating brain metastasis (assume alpha beta ratio of 10) and fractionated schemes using EQD2. This chart is provided as a quick tool and should be used in conjunction with clinical judgment with the understanding that radiobiologic modeling is an imperfect science

Table 45.6 Outcomes of hypo-fractionated treatment of brain metastases and/or surgical cavities

Series	Patients (lesions)	Lesion size (median)	Fractionation	EQD2 tumor (Gy)	Local control	Reported toxicity %
Aoyama [109]	87(159)	3.3 cc	8.75 Gy × 4	55	81%	7
Lindvall [110]	47(47)	–	8 Gy × 5	60	84%	6.25
Aoki [111]	44(65)	–	5–6 Gy × 3–5	19–30	72%	2
Fahrig [112]	150(228)	6.1 cc	6–7 Gy × 5	30–50	–	22
			5 Gy × 7	44	–	7
			10 Gy × 4	67	–	0
Narayana [113]	20(20)	–	6 Gy × 5	40	70%	15
Giubilei [114]	30(44)	2.1 cm/4.8 cc	6 Gy × 3/ 8 Gy × 4	24/48	86%	–
Kwon [115]	27(52)	1.2 cm/0.5 cc	20–35 Gy in 4–6	25–48	68%	5.8
Ogura [116]	39(46)	1.8 cm	7 Gy × 5 or	50	17%	2.5
			WBRT + 4–5 Gy × 5	31.2[a]		
Wang [117]	37(37)	Cavity > 3 cm	8 Gy × 3	36	80%	9
DePotter [118]	35(58)	8.6 cc	WBRT + 6 Gy × 5	40[a]	66%	11
Eaton et al. [119]	42(42)	3.9 cm 13.6 cc	5–8 Gy × 3–5	31–36	62%	7

[a]*BED of the hypo-fractionated course*

Hypo-fractionated treatment of brain metastasis has been reported by many authors using a wide variety of fractionation schemes and varied success and complication rates. These are summarized in Table 45.6.

Treatment Delivery

Treatment delivery can follow one of several workflow patterns depending on the fixation used and the fractionation or single session model. It is also dependent on the model of LGK being used. For brevity, we will discuss workflows with the Perfexion and Icon units.

Frame-Based SRS

The first step in the delivery of frame-based SRS on the day of treatment is the application of the Leksell stereotactic frame to the patients' head. This is performed as a clean or sterile procedure depending on the preference of the surgeon, under anxiolytics, or mild sedation in adults and general anesthesia in children. Local anesthetic is used at the four points on the scalp where the fixation screws penetrate the skin. Fixation is achieved with titanium screws (aluminum if only CT imaging will be used). Following frame application, a collision check cap is placed on the head to ensure that

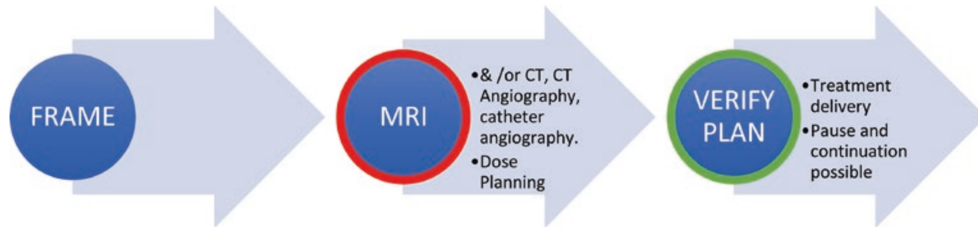

Fig. 45.17 Treatment delivery in a frame-based linear workflow. Red ring indicates image that serves as source of stereotactic coordinates, and green ring is indicative of predelivery verification

Fig. 45.18 Treatment delivery in a pre-imaging/pre-planning frame-based workflow. Orange ring indicates images that are used for getting the anatomical data for dose planning, red ring indicates image that serves as source of stereotactic coordinates, and green ring is indicative of predelivery verification

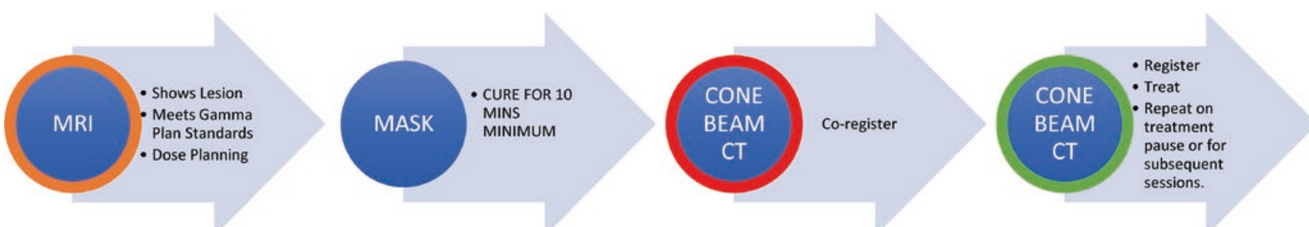

Fig. 45.19 Treatment delivery in a pre-imaging/pre-planning mask-based workflow. Orange ring indicates images that are used for getting the anatomical data for dose planning, red ring indicates image that serves as source of stereotactic coordinates, and green ring is indicative of predelivery verification

there is no risk of collision with the interior of the LGK in any desired target position.

In a linear workflow, this is followed by stereotactic MRI, CT, and catheter angiography as needed (Fig. 45.17). Since the frame limits the size of imaging coils that can be used with the MRI and the sequences that can be performed, sometimes it is preferred to perform the MRI imaging without a frame and co-registration with a frame-based CT (Perfexion), or onboard CBCT (Icon) is used to align the MRI into stereotactic space (Fig. 45.18).

Mask-Based SRS or Hypo-Fractionated SRT

Planning for mask-based treatments is performed on MRI or diagnostic CT imaging which is obtained with at least one sequence covering the whole head with a slice including air at the top and is designated as the pre-plan reference. More specialized sequences that delineate anatomy relevant to the plan can be used by co-registration with the pre-plan reference as long as the imaging covers at least a 50 mm thick slab of brain. Thermoplastic mask immobilization can be accomplished on the same day as treatment or prior to treatment. The stereotactic coordinates are obtained from the CBCT obtained at any point after the immobilization has been designed. These images are registered to the pre-plan allowing real Leksell coordinates to be acquired for the treatment plan. Prior to delivery of the actual treatment, several steps are required: (1) the HDMM (IFMM) nose marker has to be placed on the patient, (2) the HDMM camera has to be deployed, (3) the delivery fraction has to brought up on the console, and (4) one Gamma Plan station has to be in treatment mode. At this point a delivery CBCT is obtained and transferred to the Gamma Plan station in treatment mode. A co-registration window opens automatically and permits co-registration and verification of shifts. On accepting the shifts, a treatment evaluation window appears allowing the user to evaluate the influence of the repositioning on the dose plan. This can be viewed both for the current delivery as well as the cumulative delivery of all fractions delivered to that point in time. Since the shifts are applied, the comparison is made between the dynamic re-planned dose and the original plan. This workflow is illustrated in Fig. 45.19.

Quality Assurance and AAPM Task Group

Purpose

This section describes a procedure for investigating and verifying the precision of the dose delivery. Various factors may affect the dose distribution, such as the strength of each radiation source, the exact alignment to the collimator system, and the tolerances to which the collimators are manufactured.

Method

In Leksell Gamma Knife®, with very steep dose gradients and complex geometry, it is recommended to use film dosimetry because of good spatial resolution and low energy dependence. Due to the designs with a large number of sources (201 sources for Leksell Gamma Knife® B, C, 4, and 4C and 192 sources for Leksell Gamma Knife® Perfexion™ and Leksell Gamma Knife® Icon™), it is not possible to measure and investigate the beams from every single source. For Leksell Gamma Knife® B, C, 4, and 4C, the transmission through the collimator helmet would be too high, and more than 50 beams are required to have an excessive transmission of less than 1%. For Leksell Gamma Knife® Perfexion™ and Leksell Gamma Knife® Icon™, it is not possible to use only 1 beam at all, because they are designed with sectors of 24 sources each and individual sources cannot be blocked.

To investigate the precision in dose delivery, it is recommended to test the dose distributions from all beams in a standard geometry at the Leksell coordinate x,y,z = 100 mm for the various collimator sizes available on the treatment unit. The standard geometry is a sphere of 8 cm diameter. It is recommended to use the spherical phantom or the Elekta Dosimetry Phantom.

For each collimator size to be investigated:

(a) Prepare two films to the appropriate size for phantom (and collimator size).
(b) In the selected phantom type, mount the film in the center plane of the phantom in the *XY* plane.
(c) Prepare a test plan with the coordinates X, Y, Z = 100 mm, and select an appropriate dose for the film type used (e.g., 5 Gy for Gafchromic EBT type film).
(d) Expose the film to the selected dose.
(e) Repeat **steps 2–4** for the *XZ* plane.
(f) Prepare eight films to the appropriate size for phantom (and collimator size).
(g) Create a dose-intensity calibration curve.

Case Study

A 59-year-old female with known metastatic melanoma presents with short onset ataxia and mild headache. MRI of the brain reveals a hemorrhagic metastatic deposit in the R middle cerebellar peduncle. The lesion has a 9 mm solid tumor (0.3 cc) component and a 32 mm hemorrhage (7.9 cc).

Location precluded surgical removal. Given the radioresistant nature of the primary radiosurgery would be a superior method for controlling disease. Since this was a single metastasis, whole brain radiotherapy would not be appropriate. However the volume of the hemorrhage would make single session dose to this area to be restricted to reduce side effects, compromising efficacy.

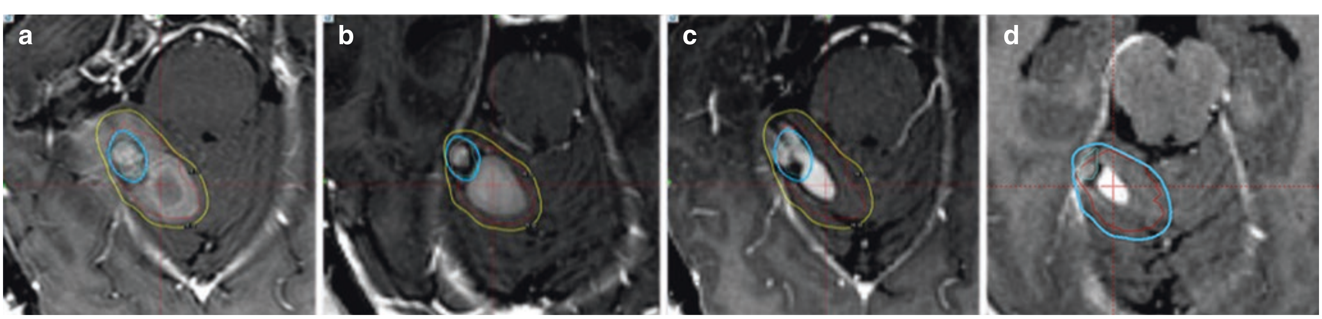

Fig. 45.20 (**a**–**d**) Metastatic melanoma with hemorrhage in the cerebellar peduncle treated with hypo-fractionated SRS showing progressive resolution of tumor and hemorrhage

Leveraging the ability to hypo-fractionate with the ICON, the entire hemorrhagic cavity was treated to15 Gy in three fractions and the solid tumor received an additional boost dose of 5 Gy. Figure 45.20 (a) shows the original plan with the hemorrhage covered by the yellow (15 Gy) line and the solid tumor portion in turquoise that received additional 5 Gy. Follow-up imaging at 2 months (b), 4 months (c), and 1 year (d) reveals resolution of hematoma and shrinkage of tumor.

Summary

Gamma Knife radiosurgery introduced the concept of radiosurgery in the CNS and has become an important tool in the management of CNS tumors in conjunction with or in lieu of microsurgery, fractionated radiotherapy, and chemotherapy. It provides the ability to deliver high doses of radiation with high precision and steep gradients for falloff in normal structures. Long-term results reflect high efficacy and low toxicity rates for the procedure. With the introduction of the ICON®, there are new indications and possibilities for the patients.

Self-Assessment Questions

1. Tolerance of the optic chiasm to single session SRS is commonly accepted to be:
   A. 12–14 Gy
   B. 2–4 Gy
   C. 5 Gy
   D. 8–10 Gy

2. Tolerance dose to the brain stem in single session SRS is
   A. 50 Gy
   B. 25 Gy
   C. 12 Gy
   D. 10 Gy

3. Gradient index refers to
   A. Homogeneity of dose inside the target
   B. Rapidity of falloff of dose in normal structures
   C. Extent of target covered in adequate dose
   D. Volume of target included in the prescription dose

4. Frame-based radiosurgery with Gamma Knife is capable of achieving a precision of
   A. Less than 2.0 mm
   B. Less than 1.0 mm
   C. Less than 0.5 mm
   D. Less than 0.1 mm

5. Dose normalization with the Gamma Knife is typically in the range of 40–70% because:
   A. It provides more choices for treatment.
   B. Minimizes treatment time.
   C. Allows more coverage.
   D. Permits optimal gradients in normal tissue.

Answers

1. D
2. C
3. B
4. C
5. D

References

1. Leksell L. The stereotaxic method and radiosurgery of the brain. Acta Chir Scand. 1951;102(4):316–9.
2. Larsson B. 1931–1998-a multidisciplinary scientist. Acta Oncol. 1999;38:389–90.
3. Paddick I, Lippitz B. A simple dose gradient measurement tool to complement the conformity index. J Neurosurg. 2006;105(Suppl):194–201. https://doi.org/10.3171/sup.2006.105.7.194.
4. Shaw E, Kline R, Gillin M, et al. Radiation therapy oncology group: radiosurgery quality assurance guidelines. Int J Radiat Oncol Biol Phys. 1993;27(5):1231–9.
5. Paddick I. A simple scoring ratio to index the conformity of radiosurgical treatment plans. Technical note. J Neurosurg. 2000;93(Suppl 3):219–22. https://doi.org/10.3171/jns.2000.93.supplement.
6. Lunsford LD, Niranjan A, Flickinger JC, et al. Radiosurgery of vestibular schwannomas: summary of experience in 829 cases. J Neurosurg. 2005;102(Suppl):195–9.
7. Regis J, Delsanti C, Roche PH, et al. Functional outcomes of radiosurgical treatment of vestibular schwannomas: 1000 successive cases and review of the literature. Neurochirurgie. 2004;50(2–3 Pt 2):301–11.
8. Landy HJ, Markoe AM, Wu X, et al. Safety and efficacy of tiered limited-dose gamma knife stereotactic radiosurgery for unilateral acoustic neuroma. Stereotact Funct Neurosurg. 2004;82(4):147–52. https://doi.org/10.1159/000081347.
9. Rowe JG, Radatz MW, Walton L, et al. Clinical experience with gamma knife stereotactic radiosurgery in the management of vestibular schwannomas secondary to type 2 neurofibromatosis. J Neurol Neurosurg Psychiatry. 2003;74(9):1288–93.
10. Iwai Y, Yamanaka K, Shiotani M, et al. Radiosurgery for acoustic neuromas: results of low-dose treatment. Neurosurgery. 2003;53(2):282–7. discussion 287-288
11. Unger F, Walch C, Papaefthymiou G, et al. Long term results of radiosurgery for vestibular schwannomas. Zentralbl Neurochir. 2002;63(2):52–8. https://doi.org/10.1055/s-2002-33975.
12. Litvack ZN, Noren G, Chougule PB, et al. Preservation of functional hearing after gamma knife surgery for vestibular schwannoma. Neurosurg Focus. 2003;14(5):e3.

13. Petit JH, Hudes RS, Chen TT, et al. Reduced-dose radiosurgery for vestibular schwannomas. Neurosurgery. 2001;49(6):1299–306. discussion 1306-1297
14. Bertalanffy A, Dietrich W, Aichholzer M, et al. Gamma knife radiosurgery of acoustic neurinomas. Acta Neurochir. 2001;143(7):689–95.
15. Prasad D, Steiner M, Steiner L. Gamma surgery for vestibular schwannoma. J Neurosurg. 2000;92(5):745–59. https://doi.org/10.3171/jns.2000.92.5.0745.
16. Liscak R, Vladyka V, Urgosik D, et al. Repeated treatment of vestibular schwannomas after gamma knife radiosurgery. Acta Neurochir. 2009;151(4):317–24.; discussion 324. https://doi.org/10.1007/s00701-009-0254-0.
17. Kwon Y, Kim JH, Lee DJ, et al. Gamma knife treatment of acoustic neurinoma. Stereotact Funct Neurosurg. 1998;70(Suppl 1):57–64.
18. Noren G. Long-term complications following gamma knife radiosurgery of vestibular schwannomas. Stereotact Funct Neurosurg. 1998;70(Suppl 1):65–73.
19. Gande A, Kano H, Bowden G, et al. Gamma knife radiosurgery of olfactory groove meningiomas provides a method to preserve subjective olfactory function. J Neuro-Oncol. 2014;116(3):577–83. https://doi.org/10.1007/s11060-013-1335-8.
20. Malik I, Rowe JG, Walton L, et al. The use of stereotactic radiosurgery in the management of meningiomas. Br J Neurosurg. 2005;19(1):13–20. https://doi.org/10.1080/02688690500080885.
21. Pollock BE, Stafford SL, Link MJ. Stereotactic radiosurgery of intracranial meningiomas. Neurosurg Clin N Am. 2013;24(4):499–507. https://doi.org/10.1016/j.nec.2013.05.006.
22. Sheehan JP, Lee CC, Xu Z, et al. Edema following gamma knife radiosurgery for parasagittal and parafalcine meningiomas. J Neurosurg. 2015;123(5):1287–93. https://doi.org/10.3171/2014.12.JNS142159.
23. Starke RM, Przybylowski CJ, Sugoto M, et al. Gamma knife radiosurgery of large skull base meningiomas. J Neurosurg. 2015;122(2):363–72. https://doi.org/10.3171/2014.10.JNS14198.
24. Wowra B, Horstmann GA, Cibis R, et al. Profile of ambulatory radiosurgery with the gamma knife system. 2: report of clinical experiences. Radiologe. 1997;37(12):1003–15.
25. Cohen-Inbar O, Lee CC, Schlesinger D, et al. Long-term results of stereotactic radiosurgery for skull base meningiomas. Neurosurgery. 2016;79(1):58–68. https://doi.org/10.1227/NEU.0000000000001045.
26. Bledsoe JM, Link MJ, Stafford SL, et al. Radiosurgery for large-volume (> 10 cm3) benign meningiomas. J Neurosurg. 2010;112(5):951–6. https://doi.org/10.3171/2009.8.jns09703.
27. Choi CYH, Soltys SG, Gibbs IC, et al. Cyberknife stereotactic radiosurgery for treatment of atypical (who grade II) cranial meningiomas. Neurosurgery. 2010;67(5):1180–8. https://doi.org/10.1227/NEU.0b013e3181f2f427.
28. Chung H-T, Kim DG, Paek SH, et al. Development of dose–volume relation model for gamma knife surgery of non-skull base intracranial meningiomas. Int J Rad Oncol Biol Phys. 2009;74(4):1027–32. https://doi.org/10.1016/j.ijrobp.2008.09.007.
29. Davidson L, Fishback D, Russin JJ, et al. Postoperative gamma knife surgery for benign meningiomas of the cranial base. Neurosurg Focus. 2007;23(4):E6. https://doi.org/10.3171/foc-07/10/e6.
30. Franzin A, Vimercati A, Medone M, et al. Neuroophthalmological evaluation after gamma knife surgery for cavernous sinus meningiomas. Neurosurg Focus. 2007;23(6):E9. https://doi.org/10.3171/foc-07/12/e10.
31. Hasegawa T, Kida Y, Yoshimoto M, et al. Gamma knife surgery for convexity, parasagittal, and falcine meningiomas. J Neurosurg. 2011;114(5):1392–8. https://doi.org/10.3171/2010.11.jns10112.
32. Jo K-W, Kim C-H, Kong D-S, et al. Treatment modalities and outcomes for asymptomatic meningiomas. Acta Neurochir. 2011;153(1):62–7. https://doi.org/10.1007/s00701-010-0841-0.
33. Kondziolka D, Mathieu D, Lunsford LD, et al. Radiosurgery as definitive management of intracranial meningiomas. Neurosurgery. 2008;62(1):53–58; discussion 58-60. https://doi.org/10.1227/01.neu.0000311061.72626.0d.
34. Massager N, De Smedt F, Devriendt D. Long-term tumor control of benign intracranial tumors after gamma knife radiosurgery in 280 patients followed more than 5 years. Acta Neurol Belg. 2013;113(4):463–7. https://doi.org/10.1007/s13760-013-0211-9.
35. Metellus P, Regis J, Muracciole X, et al. Evaluation of fractionated radiotherapy and gamma knife radiosurgery in cavernous sinus meningiomas: treatment strategy. Neurosurgery. 2005;57(5):873–86. https://doi.org/10.1227/01.NEU.0000179924.76551.cd.
36. Pollock BE, Stafford SL, Link MJ, et al. Single-fraction radiosurgery of benign intracranial meningiomas. Neurosurgery. 2012;71(3):604–612; discussion 613. https://doi.org/10.1227/NEU.0b013e31825ea557.
37. Bir SC, Ambekar S, Ward T, et al. Outcomes and complications of gamma knife radiosurgery for skull base meningiomas. J Neurol Surg B. 2014;75(06):397–401. https://doi.org/10.1055/s-0034-1376422.
38. DiBiase SJ, Kwok Y, Yovino S, et al. Factors predicting local tumor control after gamma knife stereotactic radiosurgery for benign intracranial meningiomas. International Journal of Radiation Oncology*Biology*Physics. 2004;60(5):1515–9. https://doi.org/10.1016/j.ijrobp.2004.05.073.
39. Feigl GC, Samii M, Horstmann GA. Volumetric follow-up of meningiomas: a quantitative method to evaluate treatment outcome of gamma knife radiosurgery. Neurosurgery. 2007;61(2):281–286; discussion 286-287. https://doi.org/10.1227/01.neu.0000279999.95953.ea.
40. Kano H, Park K-J, Kondziolka D, et al. Does prior microsurgery improve or worsen the outcomes of stereotactic radiosurgery for cavernous sinus meningiomas? Neurosurgery. 2013;73(3):401–10. https://doi.org/10.1227/01.neu.0000431471.64289.3d.
41. Kreil W, Luggin J, Fuchs I, et al. Long term experience of gamma knife radiosurgery for benign skull base meningiomas. J Neurol Neurosurg Psychiatry. 2005;76(10):1425–30. https://doi.org/10.1136/jnnp.2004.049213.
42. Park S-H, Kano H, Niranjan A, et al. Stereotactic radiosurgery for cerebellopontine angle meningiomas. J Neurosurg. 2014;120(3):708–15. https://doi.org/10.3171/2013.11.jns131607.
43. Park S-H, Kano H, Niranjan A, et al. Gamma knife radiosurgery for meningiomas arising from the tentorium: a 22-year experience. J Neuro-Oncol. 2015;121(1):129–34. https://doi.org/10.1007/s11060-014-1605-0.
44. Sheehan JP, Starke RM, Kano H, et al. Gamma knife radiosurgery for sellar and parasellar meningiomas: a multicenter study. J Neurosurg. 2014;120(6):1268–77. https://doi.org/10.3171/2014.2.jns13139.
45. Shin M, Kurita H, Sasaki T, et al. Analysis of treatment outcome after stereotactic radiosurgery for cavernous sinus meningiomas. J Neurosurg. 2001;95(3):435–9. https://doi.org/10.3171/jns.2001.95.3.0435.
46. Starke RM, Williams BJ, Hiles C, et al. Gamma knife surgery for skull base meningiomas. J Neurosurg. 2012;116(3):588–97. https://doi.org/10.3171/2011.11.jns11530.

47. Williams BJ, Yen CP, Starke RM, et al. Gamma knife surgery for parasellar meningiomas: long-term results including complications, predictive factors, and progression-free survival. J Neurosurg. 2011;114(6):1571–7. https://doi.org/10.3171/2011.1.jns091939.
48. Zada G, Pagnini PG, Yu C, et al. Long-term outcomes and patterns of tumor progression after gamma knife radiosurgery for benign meningiomas. Neurosurgery. 2010;67(2):322–8.; discussion 328-329. https://doi.org/10.1227/01.neu.0000371974.88873.15.
49. Zenonos G, Kondziolka D, Flickinger JC, et al. Gamma knife surgery in the treatment paradigm for foramen magnum meningiomas. J Neurosurg. 2012;117(5):864–73. https://doi.org/10.3171/2012.8.jns111554.
50. Chen Y, Li ZF, Zhang FX, et al. Gamma knife surgery for patients with volumetric classification of nonfunctioning pituitary adenomas: a systematic review and meta-analysis. Eur J Endocrinol. 2013;169(4):487–95. https://doi.org/10.1530/EJE-13-0400.
51. Ganz JC. Gamma knife treatment of pituitary adenomas. Stereotact Funct Neurosurg. 1995;64(Suppl 1):3–10.
52. Jackson IM, Noren G. Role of gamma knife therapy in the management of pituitary tumors. Endocrinol Metab Clin N Am. 1999;28(1):133–42.
53. Jagannathan J, Sheehan JP, Pouratian N, et al. Gamma knife radiosurgery for acromegaly: outcomes after failed transsphenoidal surgery. Neurosurgery. 2008;62(6):1262–9.; discussion 1269-1270. https://doi.org/10.1227/01.neu.0000333297.41813.3d.
54. Jagannathan J, Yen CP, Pouratian N, et al. Stereotactic radiosurgery for pituitary adenomas: a comprehensive review of indications, techniques and long-term results using the gamma knife. J Neuro-Oncol. 2009;92(3):345–56. https://doi.org/10.1007/s11060-009-9832-5.
55. Pomeraniec IJ, Dallapiazza RF, Xu Z, et al. Early versus late gamma knife radiosurgery following transsphenoidal resection for nonfunctioning pituitary macroadenomas: a matched cohort study. J Neurosurg. 2016;125(1):202–12. https://doi.org/10.3171/2015.5.JNS15581.
56. Thoren M, Hoybye C, Grenback E, et al. The role of gamma knife radiosurgery in the management of pituitary adenomas. J Neuro-Oncol. 2001;54(2):197–203.
57. Zeiler FA, Bigder M, Kaufmann A, et al. Gamma knife in the treatment of pituitary adenomas: results of a single center. Can J Neurol Sci. 2013;40(4):546–52.
58. Chung WY, Pan DH, Shiau CY, et al. Gamma knife radiosurgery for craniopharyngiomas. J Neurosurg. 2000;93(Suppl 3):47–56. https://doi.org/10.3171/jns.2000.93.supplement.
59. Kobayashi T, Tanaka T, Kida Y. Stereotactic gamma radiosurgery of craniopharyngiomas. Pediatr Neurosurg. 1994;21(Suppl 1):69–74.
60. Prasad D, Steiner M, Steiner L. Gamma knife surgery for craniopharyngioma. Acta Neurochir. 1995;134(3–4):167–76.
61. Ulfarsson E, Lindquist C, Roberts M, et al. Gamma knife radiosurgery for craniopharyngiomas: long-term results in the first Swedish patients. J Neurosurg. 2002;97(5 Suppl):613–22. https://doi.org/10.3171/jns.2002.97.supplement.
62. El-Shehaby AM, Reda WA, Abdel Karim KM, et al. Gamma knife radiosurgery for low-grade tectal gliomas. Acta Neurochir. 2015;157(2):247–56. https://doi.org/10.1007/s00701-014-2299-y.
63. Fuchs I, Kreil W, Sutter B, et al. Gamma knife radiosurgery of brainstem gliomas. Acta Neurochir Suppl. 2002;84:85–90.
64. Gagliardi F, Bailo M, Spina A, et al. Gamma knife radiosurgery for low-grade gliomas: clinical results at long-term follow-up on tumor control and patients' quality of life. World Neurosurg. 2017;101:540–53. https://doi.org/10.1016/j.wneu.2017.02.041.
65. Liao CH, Pan DH, Yang HC, et al. Gamma knife radiosurgery as a treatment modality for low-grade pediatric brainstem gliomas: report of two cases. Childs Nerv Syst. 2012;28(1):175–8. https://doi.org/10.1007/s00381-011-1620-9.
66. Simonova G, Novotny J Jr, Liscak R. Low-grade gliomas treated by fractionated gamma knife surgery. J Neurosurg. 2005;102(Suppl):19–24.
67. Weintraub D, Yen CP, Xu Z, et al. Gamma knife surgery of pediatric gliomas. J Neurosurg Pediatr. 2012;10(6):471–7. https://doi.org/10.3171/2012.9.PEDS12257.
68. Szeifert GT, Prasad D, Kamyrio T, et al. The role of the gamma knife in the management of cerebral astrocytomas. Prog Neurol Surg. 2007;20:150–63. https://doi.org/10.1159/0000100102.
69. Coffey RJ. Boost gamma knife radiosurgery in the treatment of primary glial tumors. Stereotact Funct Neurosurg. 1993;61(Suppl 1):59–64.
70. Elliott RE, Parker EC, Rush SC, et al. Efficacy of gamma knife radiosurgery for small-volume recurrent malignant gliomas after initial radical resection. World Neurosurg. 2011;76(1–2):128–40.; discussion 161-122. https://doi.org/10.1016/j.wneu.2010.12.053.
71. Lowell D, Tatter SB, Bourland JD, et al. Toxicity of gamma knife radiosurgery in the treatment of intracranial tumors in patients with collagen vascular diseases or multiple sclerosis. Int J Radiat Oncol Biol Phys. 2011;81(4):e519–24. https://doi.org/10.1016/j.ijrobp.2011.02.056.
72. Zeiler FA, Kaufmann AM, McDonald PJ, et al. Gamma knife radiosurgery for high grade glial neoplasms: a Canadian experience. Can J Neurol Sci. 2013;40(6):783–9.
73. Gerosa M, Nicolato A, Severi F, et al. Gamma knife radiosurgery for intracranial metastases: from local tumor control to increased survival. Stereotact Funct Neurosurg. 1996;66(Suppl 1):184–92.
74. Shiau CY, Sneed PK, Shu HK, et al. Radiosurgery for brain metastases: relationship of dose and pattern of enhancement to local control. Int J Radiat Oncol Biol Phys. 1997;37(2):375–83.
75. Kim YS, Kondziolka D, Flickinger JC, et al. Stereotactic radiosurgery for patients with nonsmall cell lung carcinoma metastatic to the brain. Cancer. 1997;80(11):2075–83.
76. Wowra B, Czempiel H, Cibis R, et al. Profile of ambulatory radiosurgery with the gamma knife system. 1: method and multicenter irradiation concept. Radiologe. 1997;37(12):995–1002.
77. Mori Y, Kondziolka D, Flickinger JC, et al. Stereotactic radiosurgery for cerebral metastatic melanoma: factors affecting local disease control and survival. Int J Radiat Oncol Biol Phys. 1998;42(3):581–9.
78. Mori Y, Kondziolka D, Flickinger JC, et al. Stereotactic radiosurgery for brain metastasis from renal cell carcinoma. Cancer. 1998;83(2):344–53.
79. Seung SK, Sneed PK, McDermott MW, et al. Gamma knife radiosurgery for malignant melanoma brain metastases. Cancer J Sci Am. 1998;4(2):103–9.
80. Chen JC, O'Day S, Morton D, et al. Stereotactic radiosurgery in the treatment of metastatic disease to the brain. Stereotact Funct Neurosurg. 1999;73(1–4):60–3.
81. Muacevic A, Kreth FW, Horstmann GA, et al. Surgery and radiotherapy compared with gamma knife radiosurgery in the treatment of solitary cerebral metastases of small diameter. J Neurosurg. 1999;91(1):35–43. https://doi.org/10.3171/jns.1999.91.1.0035.

82. Sneed PK, Lamborn KR, Forstner JM, et al. Radiosurgery for brain metastases: is whole brain radiotherapy necessary? Int J Radiat Oncol Biol Phys. 1999;43(3):549–58.
83. Lavine SD, Petrovich Z, Cohen-Gadol AA, et al. Gamma knife radiosurgery for metastatic melanoma: an analysis of survival, outcome, and complications. Neurosurgery. 1999;44(1):59–64. discussion 64-56
84. Sansur CA, Chin LS, Ames JW,et al. Gamma knife radiosurgery for the treatment of brain metastases. Stereotact Funct Neurosurg. 2000;74(1):37–51. doi:56462
85. Amendola BE, Wolf AL, Coy SR, et al. Brain metastases in renal cell carcinoma: management with gamma knife radiosurgery. Cancer J. 2000;6(6):372–6.
86. Simonova G, Liscak R, Novotny J Jr, et al. Solitary brain metastases treated with the Leksell gamma knife: prognostic factors for patients. Radiother Oncol. 2000;57(2):207–13.
87. Schoggl A, Kitz K, Reddy M, et al. Defining the role of stereotactic radiosurgery versus microsurgery in the treatment of single brain metastases. Acta Neurochir. 2000;142(6):621–6.
88. Firlik KS, Kondziolka D, Flickinger JC, et al. Stereotactic radiosurgery for brain metastases from breast cancer. Ann Surg Oncol. 2000;7(5):333–8.
89. Sheehan JP, Sun MH, Kondziolka D, et al. Radiosurgery for non-small cell lung carcinoma metastatic to the brain: long-term outcomes and prognostic factors influencing patient survival time and local tumor control. J Neurosurg. 2002;97(6):1276–81. https://doi.org/10.3171/jns.2002.97.6.1276.
90. Muacevic A, Kreth FW, Tonn JC, et al. Stereotactic radiosurgery for multiple brain metastases from breast carcinoma. Cancer. 2004;100(8):1705–11. https://doi.org/10.1002/cncr.20167.
91. Lippitz BE, Kraepelien T, Hautanen K, et al. Gamma knife radiosurgery for patients with multiple cerebral metastases. Acta Neurochir Suppl. 2004;91:79–87.
92. Mix M, Elmarzouky R, O'Connor T, et al. Clinical outcomes in patients with brain metastases from breast cancer treated with single-session radiosurgery or whole brain radiotherapy. J Neurosurg. 2016;125(Suppl 1):26–30. https://doi.org/10.3171/2016.7.GKS161541.
93. Sheehan JP, Tanaka S, Link MJ, et al. Gamma knife surgery for the management of glomus tumors: a multicenter study. J Neurosurg. 2012;117(2):246–54. https://doi.org/10.3171/2012.4.JNS11214.
94. Liscak R, Vladyka V, Simonova G, et al. Leksell gamma knife radiosurgery of the tumor glomus jugulare and tympanicum. Stereotact Funct Neurosurg. 1998;70(Suppl 1):152–60.
95. Gerosa M, Visca A, Rizzo P, et al. Glomus jugulare tumors: the option of gamma knife radiosurgery. Neurosurgery. 2006;59(3):561–9.; discussion 561-569. https://doi.org/10.1227/01.NEU.0000228682.92552.CA.
96. Chen PG, Nguyen JH, Payne SC, et al. Treatment of glomus jugulare tumors with gamma knife radiosurgery. Laryngoscope. 2010;120(9):1856–62. https://doi.org/10.1002/lary.21073.
97. Madhok R, Kondziolka D, Flickinger JC, et al. Gamma knife radiosurgery for facial schwannomas. Neurosurgery. 2009;64(6):1102–5.; discussion 1105. https://doi.org/10.1227/01.NEU.0000343743.20297.FB.
98. Sun J, Zhang J, Yu X, et al. Stereotactic radiosurgery for trigeminal schwannoma: a clinical retrospective study in 52 cases. Stereotact Funct Neurosurg. 2013;91(4):236–42. https://doi.org/10.1159/000345258.
99. Sheehan J, Yen CP, Arkha Y, et al. Gamma knife surgery for trigeminal schwannoma. J Neurosurg. 2007;106(5):839–45. https://doi.org/10.3171/jns.2007.106.5.839.
100. Phi JH, Paek SH, Chung HT, et al. Gamma knife surgery and trigeminal schwannoma: is it possible to preserve cranial nerve function? J Neurosurg. 2007;107(4):727–32. https://doi.org/10.3171/JNS-07/10/0727.
101. Kato K, Wanifuchi H, Watanabe A. Cyst formation after gamma knife radiosurgery for trigeminal schwannoma: a case report. No Shinkei Geka. 2009;37(6):573–8.
102. Kano H, Niranjan A, Kondziolka D, et al. Stereotactic radiosurgery for trigeminal schwannoma: tumor control and functional preservation. Clinical article. J Neurosurg. 2009;110(3):553–8.
103. Iikubo M, Sakamoto M, Furuuchi T, et al. A case of masticatory disturbance incidental to trigeminal schwannoma: changes in occlusal force and masticatory sensation before and after radiosurgery. Br J Radiol. 2008;81(963):e84–7. https://doi.org/10.1259/bjr/43860468.
104. Muthukumar N, Kondziolka D, Lunsford LD, et al. Stereotactic radiosurgery for jugular foramen schwannomas. Surg Neurol. 1999;52(2):172–9.
105. Pollock BE, Kondziolka D, Flickinger JC, et al. Preservation of cranial nerve function after radiosurgery for nonacoustic schwannomas. Neurosurgery. 1993;33(4):597–601.
106. Kano H, Iqbal FO, Sheehan J, et al. Stereotactic radiosurgery for chordoma: a report from the north American gamma knife consortium. Neurosurgery. 2011;68(2):379–89. https://doi.org/10.1227/NEU.0b013e3181ffa12c.
107. McTyre E, Helis CA, Farris M, et al. Emerging indications for fractionated gamma knife radiosurgery. Neurosurgery. 2017;80(2):210–6. https://doi.org/10.1227/NEU.0000000000001227.
108. Martens B, Janssen S, Werner M, et al. Hypofractionated stereotactic radiotherapy of limited brain metastases: a single-Centre individualized treatment approach. BMC Cancer. 2012;12:497. https://doi.org/10.1186/1471-2407-12-497.
109. Aoyama H, Shirato H, Onimaru R, et al. Hypofractionated stereotactic radiotherapy alone without whole-brain irradiation for patients with solitary and oligo brain metastasis using non-invasive fixation of the skull. Int J Radiat Oncol Biol Phys. 2003;56(3):793–800.
110. Lindvall P, Bergstrom P, Lofroth PO, et al. Hypofractionated conformal stereotactic radiotherapy alone or in combination with whole-brain radiotherapy in patients with cerebral metastases. Int J Radiat Oncol Biol Phys. 2005;61(5):1460–6. https://doi.org/10.1016/j.ijrobp.2004.08.027.
111. Aoki M, Abe Y, Hatayama Y, et al. Clinical outcome of hypofractionated conventional conformation radiotherapy for patients with single and no more than three metastatic brain tumors, with noninvasive fixation of the skull without whole brain irradiation. Int J Radiat Oncol Biol Phys. 2006;64(2):414–8. https://doi.org/10.1016/j.ijrobp.2005.03.017.
112. Fahrig A, Ganslandt O, Lambrecht U, et al. Hypofractionated stereotactic radiotherapy for brain metastases--results from three different dose concepts. Strahlenther Onkol. 2007;183(11):625–30. https://doi.org/10.1007/s00066-007-1714-1.
113. Narayana A, Chang J, Yenice K, et al. Hypofractionated stereotactic radiotherapy using intensity-modulated radiotherapy in patients with one or two brain metastases. Stereotact Funct Neurosurg. 2007;85(2–3):82–7. https://doi.org/10.1159/000097923.
114. Giubilei C, Ingrosso G, D'Andrea M, et al. Hypofractionated stereotactic radiotherapy in combination with whole brain radiotherapy for brain metastases. J Neuro-Oncol. 2009;91(2):207–12. https://doi.org/10.1007/s11060-008-9700-8.
115. Kwon AK, Dibiase SJ, Wang B, et al. Hypofractionated stereotactic radiotherapy for the treatment of brain metastases. Cancer. 2009;115(4):890–8. https://doi.org/10.1002/cncr.24082.

116. Ogura K, Mizowaki T, Ogura M, et al. Outcomes of hypofractionated stereotactic radiotherapy for metastatic brain tumors with high risk factors. J Neuro-Oncol. 2012;109(2):425–32. https://doi.org/10.1007/s11060-012-0912-6.
117. Wang CC, Floyd SR, Chang CH, et al. Cyberknife hypofractionated stereotactic radiosurgery (HSRS) of resection cavity after excision of large cerebral metastasis: efficacy and safety of an 800 cGy x 3 daily fractions regimen. J Neuro-Oncol. 2012;106(3):601–10. https://doi.org/10.1007/s11060-011-0697-z.
118. De Potter B, De Meerleer G, De Neve W, et al. Hypofractionated frameless stereotactic intensity-modulated radiotherapy with whole brain radiotherapy for the treatment of 1-3 brain metastases. Neurol Sci. 2013;34(5):647–53. https://doi.org/10.1007/s10072-012-1091-0.
119. Eaton BR, Gebhardt B, Prabhu R, et al. Hypofractionated radiosurgery for intact or resected brain metastases: defining the optimal dose and fractionation. Radiat Oncol. 2013;8:135. https://doi.org/10.1186/1748-717X-8-135.